

Experimental tests on the limit states of dry-jointed tuff blocks

Claudia Casapulla · Francesco Portioli

Received: 13 July 2014 / Accepted: 19 January 2015 / Published online: 28 January 2015
© RILEM 2015

Abstract A proper definition of the yield domains governing the frictional behaviour at contact interfaces is generally required to perform the limit analysis of 3D dry-jointed masonry block structures. However, the modelling of the actual behaviour of frictional contact interfaces under simultaneous normal and shear forces, torsion and bending moments is a topic still poorly studied, especially from the experimental point of view. In this paper the single contact interface of a system composed of two dry-jointed tuff blocks under different loading conditions is experimentally investigated. The programme includes several sets of tests based on different eccentricities of the vertical and horizontal loading implying pure strengths and interactions among shear, torsion and bending moments. The results of each set are then compared with those obtained by a recently proposed numerical model for 3D masonry block assemblages, based on the assumptions of infinite strength in compression, tension and shear for blocks and no-tension and frictional behaviour at their contact. The comparison is useful, on the one hand, as a further validation the efficacy of the previously proposed yield domains in order to be used in 3D limit

analysis formulations and, on the other, to highlight which yield domains need to be better represented.

Keywords Experimental frictional behaviour · Limit state analysis · 3D dry-jointed masonry block structures · Torsion strength · Torsion–shear–bending moment interaction effects · Non-linear yield criteria

1 Introduction

It is well known that limit state analysis simplifies and gives enough relation into the load capacity and collapse mechanism of engineering structures, with a reduced number of material parameters necessary to perform the analysis. This tool is particularly interesting for seismic analysis of masonry buildings which do not conform to box behaviour because of lack of stiff floor slabs or because of weaker partial collapses affecting the façade or inner walls.

A modelling strategy, which has demonstrated to be useful in the limit analysis of masonry structures, is the combination of block elements, rigid or deformable, with interface elements, especially when frictional behaviour is considered.

The application of rigid block limit analysis to masonry structures has received a growing attention from researchers in the last decades [5–9, 22, 23, 30, 31]. Of particular interest are the formulations of the problem in terms of mathematical programming

C. Casapulla (✉) · F. Portioli
Department of Structures for Engineering and
Architecture, University of Naples Federico II, via Forno
Vecchio 36, 80134 Naples, Italy
e-mail: casacla@unina.it

[2, 3, 14, 15, 25, 27, 29]. Within these approaches the blocks are treated as nodes and the interfaces as elements of a conventional finite element discretization (discrete element modelling). Failure modes are defined as sets of relative displacements among blocks at their contact interfaces and, when the blocks are assumed to possess infinite compressive strength, they generally involve separation, rocking, sliding and twisting of the interfaces, and combinations of them. Cracking, crushing or deformation of the elements are generally ignored, unless different material models for rigid-body elements are considered [28].

Crucial to the model formulation is a proper description of the constitutive laws that govern the contact behaviour. In direct analogy to plasticity, a set of yield conditions delineating contact failure can be defined in the space of the static variables, as the failure modes behave in essentially a rigid perfectly-plastic manner [12, 17, 19]. The contact forces are normal and shear forces as well as bending and torsion moments, corresponding in a virtual work sense to the internal degrees of freedom of the contact interface.

However, the definition of the yield domains and their interactions to properly describe potential three-dimensional responses of dry assemblages of rigid blocks still represents a hard task, as the modelling of the actual behaviour of frictional contact interfaces under simultaneous shear forces, torsion and bending moments is a topic still poorly studied [7, 25, 32], especially from the experimental point of view. In fact, large attention has been paid in the past only to the characterization of the shear behaviour of frictional contacts. In the 1960s and 1970s of the last century, a number of experimental investigations were carried out on rock friction, mostly to simulate the earthquake fault slips, e.g., those reported by Byerlee [4]. These were particularly devoted to study the variables that may affect the details of frictional response, i.e., surface roughness, magnitude of pressure, slip velocity and other. Also, the unstable frictional sliding was experimentally represented by the stick-slip behaviour. An historical review on this topic was presented by Feeny et al. [13]. However, these studies were only interested in the definition of the initial shear strength and thereafter the Coulomb's law was considered the most adequate in practice, also for rigid body mechanics. Several test methods to determine the strength parameters of masonry structures were investigated [1, 11, 16, 21, 24, 33, 34] and the triplet

test was then adopted as the standard test in Europe, CEN [10]. No standard tests are instead available for torsion–shear–bending moment interactions.

Furthermore, it should be noted that most 3D limit analysis formulations developed to date have been validated against results from in-plane loaded wall panels [22], due to the scarcity of experimental data covering other loading scenarios [26, 30, 36].

As a first attempt to fill such a gap of information, this paper presents an experimental investigation on 3D yield domains and their interactions, with reference to the single contact interface of a system composed of two dry-jointed tuff blocks. The experimental programme includes several sets of tests based on different eccentricities of the vertical and horizontal loading implying interactions among shear, torsion and bending moments. The results of each set are then compared with those obtained by the numerical model presented in [27], based on the assumptions of infinite strength in compression, tension and shear for blocks and no-tension and frictional behaviour at their contact.

2 Experimental investigation

A series of experimental tests were carried out to investigate the 3D frictional behaviour of dry masonry joints. Specimens were made of stacks formed of two dry-jointed tuff blocks with dimensions of $300 \times 200 \times 100$ mm and weight of 75 N each. The units were previously sawn in mechanical cutting. Various yield conditions in 3D masonry assemblages were considered adopting different combinations of axial and shear forces as well as torsion and bending moments. The testing device was designed and realized ad hoc since no standard equipments and procedures were found in the literature.

2.1 Test setup

The tests on the specimens of two overlapped tuff blocks were carried out using a universal electromechanical testing machine (Galdabini SUN 5), as illustrated in Fig. 1a.

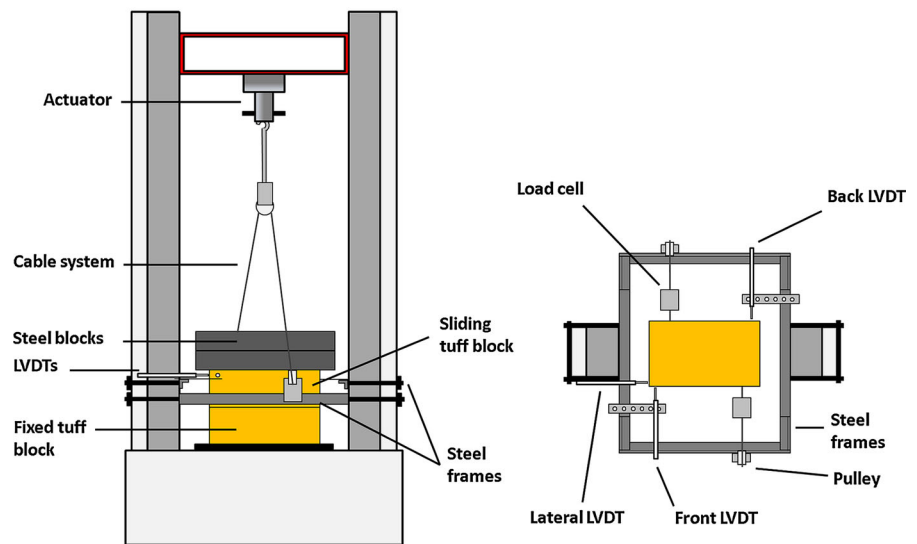
The loading system was conceived in order to transfer both a constant vertical force with varying eccentricity and variable horizontal forces on the surface between the two blocks, so as to induce sliding



Fig. 1 a The testing machine. b Test setup



(a)



(b)

failure under increasing shear forces and/or torsion moments on the same surface.

To this aim, external vertical and horizontal loads were only applied to the upper block, whereas the block at the base was fixed with a timber frame at the testing machine (Fig. 1b). The constant vertical load was applied at different eccentricities using two steel blocks with dimensions of $360 \times 135 \times 600$ mm and weight of 196 N each. The two steel blocks were simply placed one over the other on the top of the

upper tuff block and no fixing devices were required as the steel blocks were not subject to any other loading. In fact, to activate the failure mechanism at the dry joint interface between the tuff blocks, monotonically increasing horizontal forces were only applied to the side faces of the upper block, by means of eye bolts fixed on specific points at half of the block's height.

To apply the loads on the tuff block along the horizontal plane, a steel cable supported by a system of small pulleys and a steel frame was connected to the

actuator of the testing machine running in the vertical direction. The load was applied under displacement control at a constant rate of 10 mm/min.

The forces were measured using two load cells with a maximum capacity of 500 N and an acquisition frequency of 10 Hz, positioned between the cable and the tuff block. The displacements were measured using three linear variable displacement transducers (LVDTs) with a displacement range of ± 50 mm supported by the steel frame. The LVDTs were positioned at the edges of the blocks in order to detect the activation of failure mechanism and measure three independent components of displacements to obtain the translation and rotation of the sliding block. As the kinematics of the failure is beyond the scope of this paper, only the results of the front and back LVDTs are reported in the following sections.

The actual joint behaviour of two rough blocks passing over each other is strongly dependent on surface roughness, as already highlighted by Byerlee [4]. In fact, the difficulty to define the exact friction coefficient for rock materials at low normal stresses is mainly due to a large scatter in the data which can be reduced by increasing pressure on the contact surface.

Therefore, to limit the dispersion, an additional vertical loading was added, the contact surface was accurately dusted with compressed air before each test and a limited number of five tests for each set were carried out.

Despite a still low pressure level (of about 0.1 MPa), coefficients of variation (CVs) smaller than 3 % for shear tests and up to about 6 % for other tests were registered, as detailed in Sect. 3. It is expected that increasing the normal force the scatter in the data would be further reduced and the pure shear force would increase according to the Coulomb friction law [21].

2.2 Testing programme

The experimental programme was planned in order to analyze the influence of the following parameters on the bed joint response: the eccentricity of the vertical and horizontal loading implying interactions among shear, torsion and bending moments.

Figure 2 shows the two overlapped blocks and their bed joint referred to axes X , Y and Z of the standard Cartesian coordinate system in three dimensions. The block dimensions $a \times b \times h$ are $300 \times 200 \times 100$ mm, the normal force on the bed joint is given

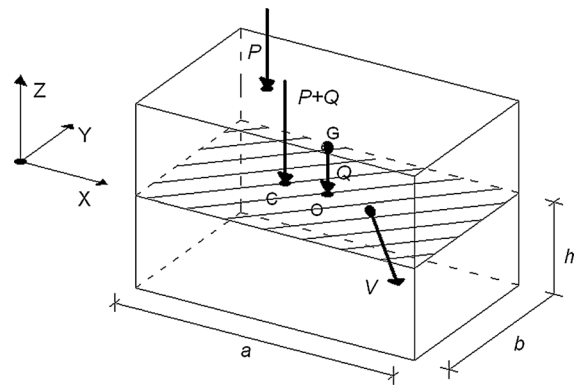


Fig. 2 Vertical and horizontal loading on the tested specimen of two overlapped blocks

by the sum of the weight of the upper block ($Q = 75$ N) and the overload ($P = 392$ N) applied on the top at a variable eccentricity from the centre of gravity G . The application point of this resultant force ($P + Q$) on the contact surface is the centre of compression C . The horizontal loading is represented either by the shear force V applied at variable eccentricity and direction in the midplane of the upper block or by a pair of shear forces in Y -direction applied at symmetric points with respect to the YZ -plane containing G and O .

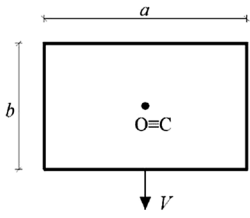
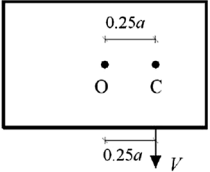
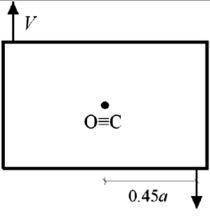
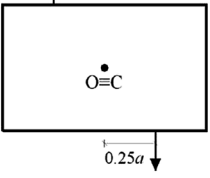
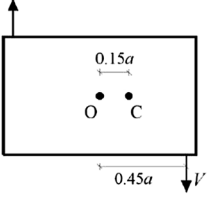
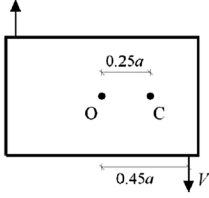
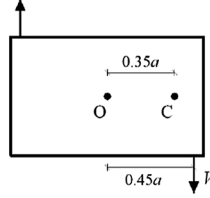
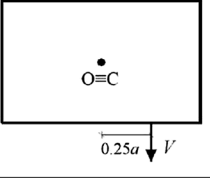
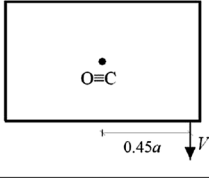
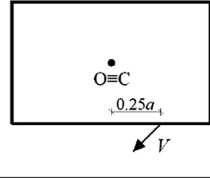
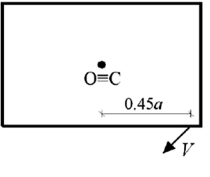
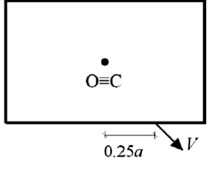
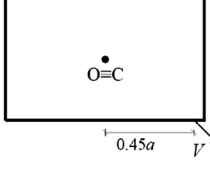
Five different series were tested, which differ both for vertical and horizontal loading conditions. Each series included a number of 5 tests, with the exception of the shear testing for which 10 tests were carried out. A total of 125 tests were performed. Tables 1 and 2 gather all the experimental cases represented in the XY -plane of the bed joint.

In the first series, the pure shear failure was achieved in two sets (Sets 1a, b) implying the condition that the resultant normal stress on the contact interface and the applied horizontal force belonged to the same vertical plane, so that no torsion moment could arise on the contact interface.

In the second series, the pure torsion failure was achieved by applying a centred overload and a pair of horizontal forces to the weighting block in its midplane and symmetrically to vertical midplane (Sets 2a, b). Two different level arms of the couple were considered.

In the third series the interaction between the torsion failure and the bending moment was investigated. In fact, a pair of horizontal forces was applied to the upper block in its midplane, in combination with a

Table 1 Experimental series for 3D yield domains of frictional bed joints

Yield	Set			
	1a)	1b)		
Pure Shear				
	Pure Torsion			
Torsion-bending moment				
	Torsion-shear			
				

Sets 1a–4f

Table 2 Experimental series for 3D yield domains of frictional bed joints

Yield	Set		
	5a)	5b)	5c)
Torsion-shear-bending moment			
	5d)	5e)	5f)
	5g)	5h)	5i)
	5j)	5k)	5l)

Sets 5a–l

vertical overload with some eccentricity from the block centre of gravity. Three conditions of small, medium and large eccentricity of the resultant vertical load were considered (Sets 3a–c).

In the fourth series the torsion–shear interaction was developed through the application of a centred vertical loading and different horizontal load conditions corresponding to various application points and orientations of the force (Sets 4a–f).

The last series is referred to several combinations of the previous loading conditions, so that interactions

among torsion, shear and bending moment could be analyzed all together (Sets 5a–l).

3 Experimental results

3.1 Friction coefficient and pure shear strength

The friction coefficient for two overlapped tuff bricks was measured through two sets of five tests implying pure shear failure of the bed joint. Both sets involved

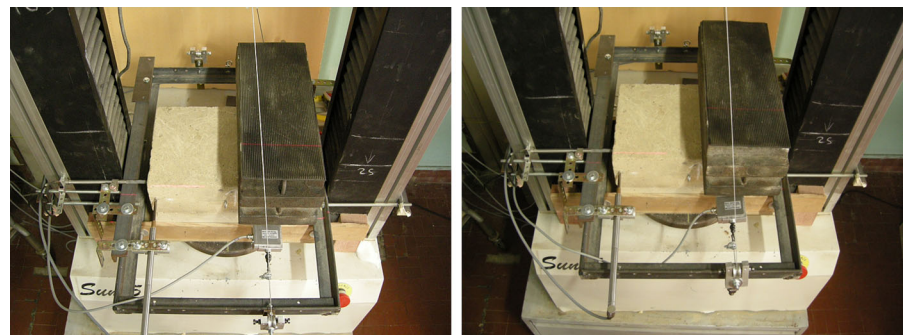
the condition that the resultant normal stress on the contact interface and the applied horizontal force lie on the same vertical plane, so that no torsion moment could arise (Fig. 3). In fact, for the first Set 1a the centre of compression C coincides with the projection of G on the contact interface in the XY -plane, say point O (Fig. 2), and the shear stresses due to the horizontal force centrally applied at the upper block is likely to be uniformly distributed on the whole contact surface. It should be mentioned that, whatever the loading arrangements can be used for the testing setup, it is not possible to provide fully uniform normal and shear stresses along the joint so that failure occurs simultaneously at all points of the joint [18]. However, pure displacement takes place if the alignment of the resultant of shear stresses and the external shear force is provided (C is also the shear centre).

In case of eccentric vertical loading (outside of the central core of inertia of the contact surface), i.e., for Set 1b, the resistant contact area tends to reduce because of a sort of partialization of the contact surface (no tensile strength). For this set, it was observed that applying the horizontal force on the Y - Z plane containing point C , only pure

displacement in Y -direction occurred (see the red laser lines in Fig. 3a, b). This means that no torsion moment takes place whatever the distribution of the normal and shear stresses on the reduced area and that, also in this case, the resultant of shear stresses is aligned with the external shear force (here too, C coincides with the shear centre). This experimental evidence can be considered as a validation of the assumption of a “reduced effective area” with centroid in C , introduced by Casapulla and D’Ayala [7] for the evaluation of torsion–bending moment interaction, as also highlighted in Sect. 3.3 and briefly recalled in Sect. 4.

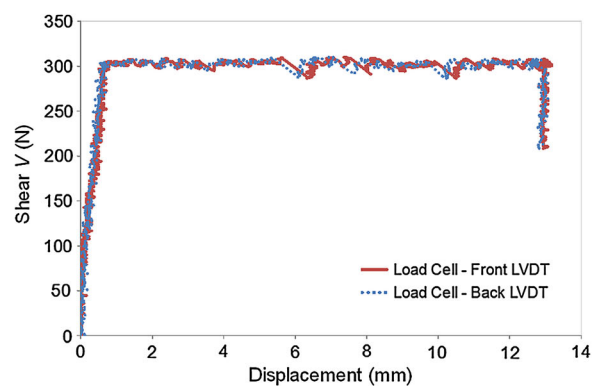
The first set of five tests (Set 1a) was carried out by putting the overload $P = 392$ N centred on the top block and by applying the horizontal force at the centre of gravity of the same block (point G in Fig. 2). For the second set of five tests (Set 1b) the horizontal force was applied at the eccentricity of $0.25a$ and the overload was placed at the eccentricity of about $0.3a$, so that the eccentricity of $0.25a$ resulted for the centre of compression C on the contact surface, as well. The overload was placed symmetrically with respect to the XZ -midplane in both cases.

Fig. 3 Friction test (Set 1b). Sample under eccentric vertical load: **a** before testing, **b** after testing, and **c** load–displacement curves



(a)

(b)



(c)

In Fig. 3c one of the five tests of Set 1b is plotted in terms of load–displacement and in Table 3 the data are reported in terms of the friction coefficient (mean, minimum and maximum values) and the CV.

The horizontal force registered by the load cell was combined with the displacements registered both by the front LVDT (red continuous line) and by the back LVDT (blue dotted line) in *Y*-direction, taking into account that the former transducer works in compression while the latter in tension. As expected, the signals registered by both LVDTs are almost coincident, with an almost vertical branch representing the rigid behaviour of the block interface and their maximum value occurring at the first noticeable movement. The displacements registered after this point show the aforementioned stick-slip behaviour which is typical of frictional sliding. However, it is worth noting that the enhancement of displacement occurred without increasing of the loading force.

The maximum force is considered as the reference pure shear strength and the friction coefficient is obtained by means of the cohesion-less Coulomb's law, i.e.,

$$\mu = \frac{V_0}{N}, \quad (1)$$

where V_0 and N are the limit shear strength and the normal force at the contact interface, respectively.

On the other hand, it is evident from the results summarized in Table 3 that the mean friction coefficient is independent of the eccentricity of the applied loads (Sets 1a, b), provided that a pure shear failure is activated. The low variability between the minimum and the maximum values and the small CVs obtained imply that the correspondent mean values are reliable enough to be used for the numerical analysis. The value used in numerical investigation is therefore $\mu = 0.64$ and the experimental pure shear strength according to the cohesion-less Coulomb's law is $V_0 = 297.8$ N, being $N = 467$ N.

Table 3 Experimental friction coefficient

μ	Mean	CV (%)	Min	Max
Set 1a	0.64	2.09	0.62	0.65
Set 1b	0.65	2.98	0.63	0.68
Total set (10 tests)	0.64	2.57	0.62	0.68

In order to validate the innovative experimental device, these results were compared with the results from direct shear tests conducted on couplet specimens available in the literature.

Firstly, the shape of the load–displacement curves is in good agreement with the findings of Vasconcelos and Lourenço [34]. In fact, the monotonic tests conducted on dry granitic blocks showed a similar non-linear branch in the presliding phase and a plateau after peak stress, representing the considerable plastic deformations associated to inelastic sliding. The stick-slip phenomenon is less pronounced than that observed in Fig. 3c, probably due to the larger normal forces applied. Also, no shear softening/hardening was recorded after peak stress. These results indicate the rather rigid-plastic behaviour of the joints.

Secondly, although a unique value of the normal force was considered in this paper, it is expectable that the shear strength will vary with different normal forces according to cohesion-less Coulomb friction law. In fact, the validity of the Coulomb failure can be lost at high normal force, while guaranteed for moderate stress levels [21].

Lastly, the friction coefficient of dry tuff joints presented in this paper ($\mu = 0.64$) is similar to the values found by Vasconcelos and Lourenço [34] for granitic units ($\mu = 0.65$), by Lourenço and Ramos [21] for sandstone joints ($\mu = 0.63$), and by Lee et al. [20] for granitic units ($\mu = 0.69$). The narrow range of values found for the friction coefficient seems to indicate that no significant differences are expected among distinct types of natural stone under similar roughness surface conditions (sawn-cut surfaces). However, the experimental results presented by Villemus et al. [35] also demonstrated that the friction coefficient is independent of the roughness surface of the blocks.

3.2 Pure torsion strength

In order to determine the pure torsion strength, the experimental equipment described above was used and a pair of horizontal forces in *Y*-direction was applied at specific points of the weighting block, symmetrically to *YZ*-midplane (Figs. 1a, 2). Two different arms of the couple were considered, i.e., $0.9a$ for Set 2a and $0.5a$ for Set 2b, while the overload was placed centred on the top block ($O \equiv C$).



Figure 4 shows two load–displacement curves plotted for one of the five tests of Set 2a. The one in red continuous line is referred to the front point of loading and the back point of displacement, while that in blue dotted line represents the other symmetric points of loading and displacement.

Both curves highlight a “hardening” branch after the rigid behaviour, instead of the constant loading observed for the previous tests. This effect can be explained by a kinematical point of view, at least partially. In fact, it should be observed that the more the displacement increases, the shorter the level arm of the applied couple is provided. This means that the forces should increase to achieve the same pure torsion strength, though no longer perpendicularly to the face of the block. It will be shown later in the text that also the combinations of loading with torsion moment may relatively be affected by the same effect. Instead, slight differences between the two curves may be a result of geometric imperfections in the experimental specimens. However, the force corresponding to the first displacement was considered as the reference resistance.

The torsion strength M_{T0} was simply obtained as the moment caused by the applied forces V about the centroid of the contact interface O or the product of the force and the corresponding lever-arm distance, as well. The results for Sets 2a and b are reported in Table 4.

It is evident in this table that the pure torsion strength is almost the same for the two sets of test, whilst the shear forces increase with decreasing lever-arms, as expected. Also the low variability of the

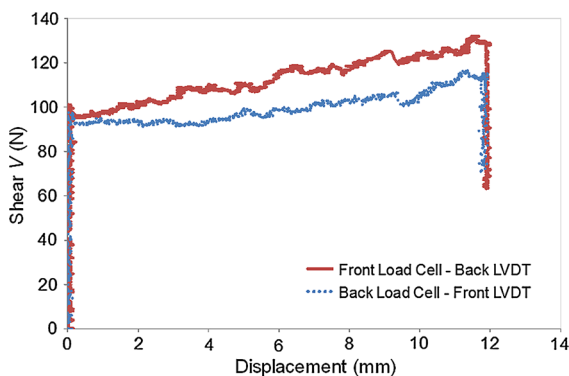


Fig. 4 Load–displacement curves for pure torsion test (Set 2a)

results (CV up to 5.07 %), implies a good reliability of the tests.

3.3 Torsion moment under eccentric normal loading

The effect of the bending moment on the torsion strength was experimentally investigated through the application of the given vertical loading at some eccentricity from the centre of gravity and of a pair of horizontal forces in Y -direction at symmetric fixed points of the weighting block (Fig. 5a). Three conditions of small, medium and large eccentricity of the resultant vertical load were considered, as reported in Table 5.

Figure 5b shows the two load–displacement curves plotted for one of the five tests of Set 3b. It is worth noting that the trend of increasing shear forces after the first movement was similar to that already observed in Fig. 4, meaning that it may be affected by the same effect described above. Also, the back LVDT reported displacements smaller than those reported by the front one because the centre of torsion is expected to be coincident with the centre of compression and, hence, closer to the back transducer, as well explained in Portioli et al. [27].

On the other hand, the results in Table 5 show that the mean shear force V and torsion moment M_{T0} decrease with increasing eccentricity of the centre of compression. This is due to the fact that the eccentric loading will reduce the resistant contact surface, so that an effective reduced area can be considered for the evaluation of torsion–bending moment interaction [7, 27]. The CVs are of the same order of magnitude as for the previous tests.

3.4 Torsion–shear interaction

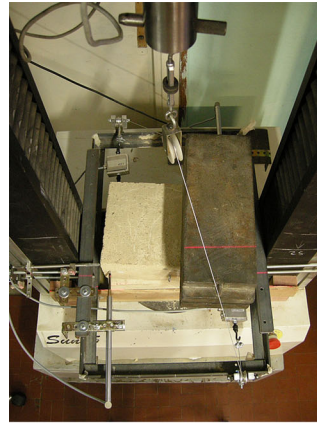
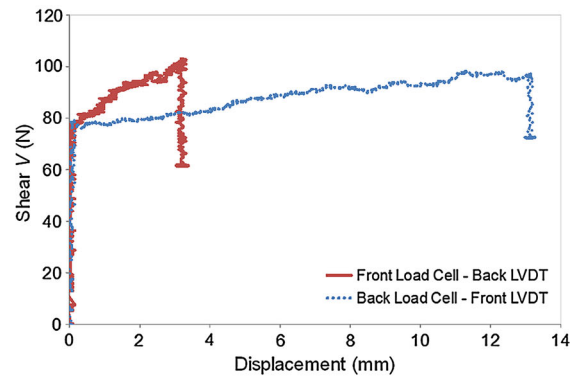
Different horizontal load conditions under centred vertical loads ($O \equiv C$) were applied to define the torsion–shear interaction experimentally. A single horizontal force was applied in the midplane of the upper block and two groups of sets were investigated (Fig. 6a). The first group includes the cases of the shear force parallel to the Y -axis and applied at two different points (Sets 4a, b), while the second group is referred to the shear force inclined by an angle of $\pm 45^\circ$ to the same axis and applied at the same different points (Sets 4c–f). The experimental results are

Table 4 Experimental pure torsion strength

	Mean V (N)	Mean M_{T0} (Nm)	CV (%)	Min V (N)	Max V (N)
Set 2a	108.2	29.2	4.11	102.8	114.2
Set 2b	205.4	30.8	5.07	196.2	221.5

Fig. 5 Torsion–bending moment test (Set 3b).

a Sample under eccentric vertical load and horizontal coupled forces, and **b** load–displacement curves

**(a)****(b)****Table 5** Experimental torsion–bending moment interaction

	Mean V (N)	Mean M_{T0} (Nm)	CV (%)	Min V (N)	Max V (N)
Set 3a	96.1	25.9	4.25	91.3	100.1
Set 3b	82.5	22.3	5.84	76.4	87.3
Set 3c	66.4	17.9	1.80	65.0	68.1

gathered in Table 6, where V and M_T are represented by their absolute values.

Figure 6b shows the two load–displacement curves plotted for one of the five tests of Set 4b. The trend of increasing shear forces after the first movement was again similar to that already observed in Figs. 4 and 5. However, in this case, the displacements at the back LVDT were greater than those at the front one because the centre of torsion is expected to be on the opposite side with respect to the YZ -midplane of the block and, hence, closer to the front point. This is consistent with the motion of the block which is characterized by a rotation about a centre away from the centre of gravity.

According to this, the results in Table 6 show that increasing the eccentricity, the torsion moment will increase and the shear force decreases. The variability of the results is still relatively low, with a CV ranging from 2.67 % up to 5.96 %.

3.5 Torsion–shear interaction under eccentric normal loading

The effects of the bending moments on the torsion–shear interaction were experimentally investigated by testing a number of load combinations (Fig. 7), as reported in Table 7. V and M_T are still represented as their absolute values, taking into account that M_T is referred to the moment of V around point O.

The load–displacement curves for these sets have trends similar to those already observed and also in these cases the variability of the results is relatively limited, ranging up to 6.8 %.

One of the most interesting remarks is that the shear force applied at a given point with little distance from the centre of compression was for all cases much greater than the force applied at the same point and with the same direction but with larger distance from

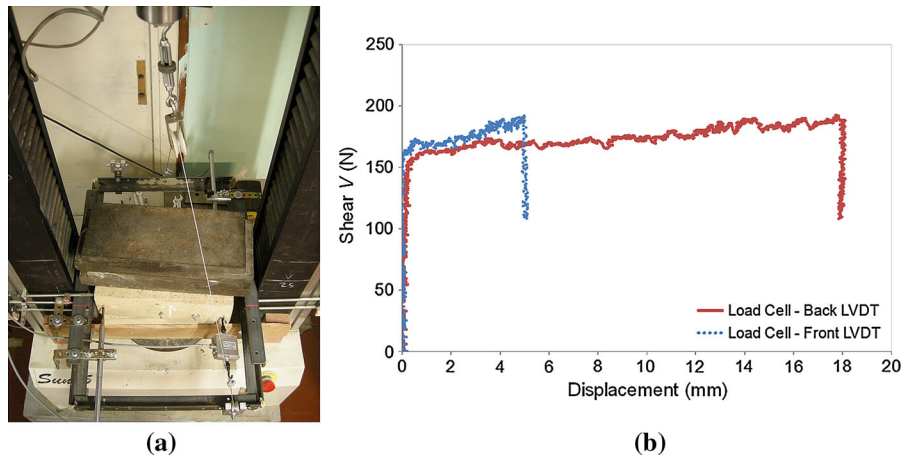


Fig. 6 Torsion–shear test (Set 4b). **a** Sample under centred vertical load and eccentric horizontal force, and **b** load–displacement curves

Table 6 Experimental torsion–shear interaction

	Mean V (N)	Mean M_T (Nm)	CV (%)	Min V (N)	Max V (N)
Set 4a	216.3	16.2	2.67	209.4	224.5
Set 4b	165.7	22.4	3.18	160.3	172.4
Set 4c	176.2	21.8	3.64	169.3	183.1
Set 4d	147.1	24.4	5.82	136.2	157.2
Set 4e	294.1	5.2	5.96	278.3	324.2
Set 4f	285.2	7.1	5.17	264.8	303.3

C. This trend can be observed by comparing some sets taken in pairs, i.e., Sets 5c versus 5d, 5e versus 5f, 5g versus 5h, 5i versus 5j and 5k versus 5l.

Consider for example Sets 5e and f shown in Fig. 7, where the sample is subjected to the eccentric horizontal force inclined of 45° and to the eccentric vertical load on the right and left side, respectively. In the first case (Set 5e) the shear force, which is very close to the centre of compression, is larger of about 80 % than the force required to move the block when the vertical load is far from it (Set 5f).

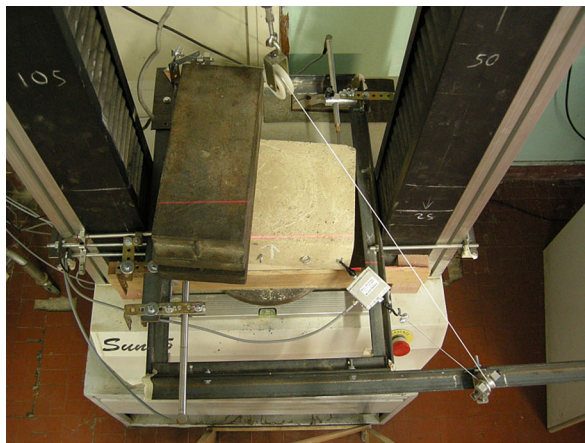
Although the kinematics of the failure is beyond the scope of this paper, it is interesting to note that also the position of the centre of torsion is affected by this distance. In fact, the load–displacement curves for Set 5e (Fig. 7) show that, while the shear force increases, the displacements registered by the two LVDTs also increases, one slightly less than the other. This means that the centre of torsion is not far from the centroid of the contact interface, though shifted to the left. Instead, when the vertical loading is placed at the opposite side of the shear force with respect to the YZ -midplane of the

block, i.e. for Set 5f, the displacement of the front LVDT is practically zero, while the other increases. In this case the centre of torsion is further away from the centroid O on the left side, very close to the front point.

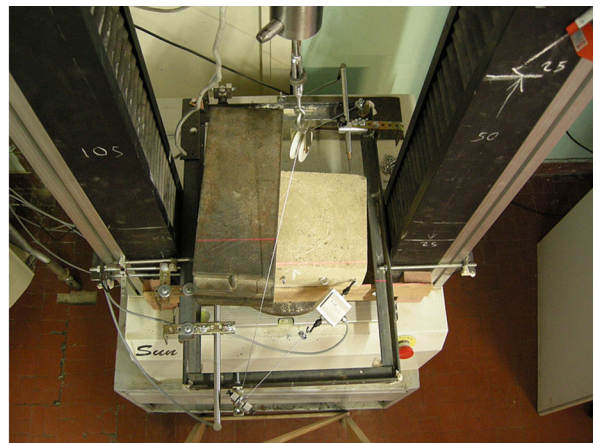
However, this remark also confirms the fact discussed above that when the shear force is applied in a vertical plane very close to the centre of compression—coincident with the shear centre—the failure tends to a pure shear type, e.g., Sets 5c, j, k for which the force is close to the shear strength.

4 Experimental versus numerical results

The yield functions for each failure mode and their combinations defined in Portioli et al. [27] are herein applied to the single frictional contact interface between two rigid blocks modelling the sample experimentally analyzed above. The results of linear/linearized and non-linear formulations are compared with the experimental ones in terms of limiting shear force, as reported in Table 8.



Set 5h)



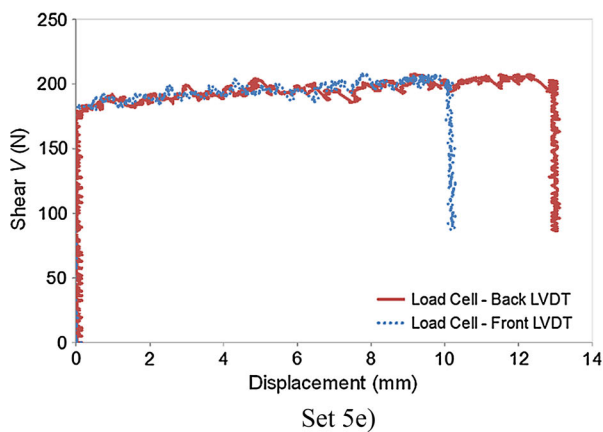
Set 5l)



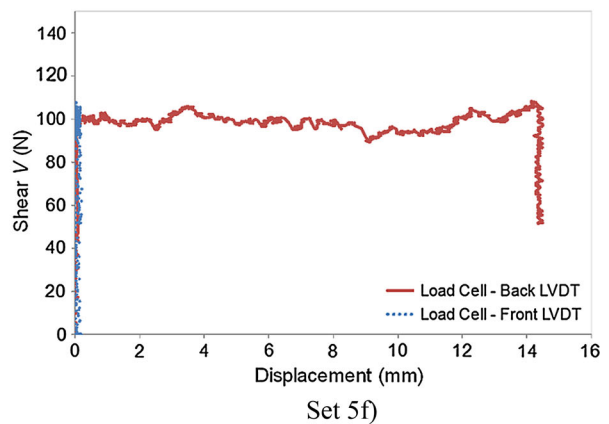
Set 5e)



Set 5f)



Set 5e)



Set 5f)

Fig. 7 Torsion–shear–bending moment test (Sets 5e, f, h, l). Sample under eccentric vertical load and eccentric horizontal force (inclined of $\pm 45^\circ$). Load–displacement curves for Sets 5e, f)

According to the adopted model, failure is concentrated at the centre point of the block interface and includes different types of collapse modes, namely

joint separation, rocking, sliding and twisting, and combinations of them. The blocks are considered infinitely strong in compression, tension and shear so

Table 7 Experimental torsion–shear–bending moment interaction

	Mean V (N)	Mean M_T (Nm)	CV (%)	Min V (N)	Max V (N)
Set 5a	190.5	0.0	4.08	180.1	208.2
Set 5b	122.4	9.2	2.78	116.5	127.7
Set 5c	207.7	28.0	6.80	191.8	241.5
Set 5d	91.4	12.3	2.69	85.2	94.3
Set 5e	188.6	23.3	2.24	183.0	199.1
Set 5f	105.6	13.1	1.42	103.5	108.5
Set 5g	151.9	25.2	2.58	145.1	158.3
Set 5h	85.4	14.2	3.67	80.5	91.2
Set 5i	189.6	3.3	5.87	166.8	211.7
Set 5j	241.2	4.3	1.68	233.5	248.8
Set 5k	253.3	6.3	4.34	242.4	282.5
Set 5l	186.0	4.6	3.48	179.2	201.4

that no crushing/cracking and no deformation can take place. Also, no-tension behaviour and infinite compressive strength are assumed for the frictional contact.

The yield functions of contact static variables are represented by the internal forces acting at interface and referred to the centre of contact (Fig. 8a), i.e., the two components of the shear force V (V_1 and V_2) and of the bending moment M (M_1 and M_2), the normal force N and the torsion moment M_T . The contact forces correspond in a virtual work sense to the internal degrees of freedom of the contact interface.

As well described in the cited work, the pure shear strength was represented by a piecewise linearized cohesion-less Coulomb's cone, while the pure torsion moment strength was expressed by a linear yield function of the shear strength or normal force. These diagrams are represented in Fig. 8b, c in the positive quadrant only.

These yield functions, simplified to be applied to the sample, are, respectively:

$$y^s = \sqrt{V_1^2 + V_2^2} - V_0 \leq 0, \quad (2)$$

$$y^t = |M_T| - M_{T0} \leq 0, \quad (3)$$

where:

$$M_{T0} = V_0 c_T \quad V_0 = \mu N, \quad (4)$$

being c_T the torsion constant and $\mu = 0.64$ the value of the friction coefficient.

In case of torsion–shear interaction, a non-linear formulation can be derived according to Casapulla [5],

as represented in Fig. 8d. However, the conservative linear approximation sketched in the same figure was considered in Portioli et al. [27] in order to reduce the 3D limit analysis problem to a linear program. It can be expressed by the relation:

$$y^{ts} = |M_T| - M_{T0} \left(1 - \frac{V}{V_0}\right) \leq 0. \quad (5)$$

Instead, the torsion–bending moment interaction was based on the assumption of a reduced effective contact interface [7]. The yield function associated with this failure criterion is:

$$y^{tb} = |M_T| - M_{T0,eff} \leq 0, \quad (6)$$

where:

$$M_{T0,eff} = V_0 c_{T,eff}, \quad (7)$$

being $c_{T,eff}$ the torsion constant calculated with reference to the reduced contact interface. The torsion strength $M_{T0,eff}$ decreases as the bending moments increase through a slightly non-linear relationship, as shown in Fig. 8e considering $M_1 = 0$. In particular, point A represents the condition $M_2/M_{2,0} = 1$ for which the torsion strength is not equal to zero but it assumes the value [27]:

$$M_{T0,eff}^A = \frac{1}{4} V_0 b. \quad (8)$$

The yield domain derived by this assumption, also used by Orduña and Lourenço [25], implies an ad hoc iterative procedure because in 3D block assemblages the eccentricities of the normal forces at contact

Table 8 Comparison of experimental and numerical results

Yield	Sets	Exp V (N)	Non-linear V (N)	Linear/linearized V (N)	Diff. linear/non-linear versus exp. (%)
Pure shear	1a	297.8	–	298.9	–0.36
	1b	302.6	–	298.9	–1.22
Pure torsion	2a	108.2	–	107.2	–0.96
	2b	205.4	–	192.9	–6.08
Torsion–bending moment	3a	96.1	86.8	–	–9.62
	3b	82.5	74.6	–	–9.61
	3c	66.4	64.1	–	–3.45
Torsion–shear	4a	216.3	–	168.4	–22.13
	4b	165.7	–	124.8	–24.67
	4c	176.2	–	131.2	–25.53
	4d	147.1	–	110.0	–25.21
	4e	294.1	–	252.7	–14.08
	4f	285.2	–	238.0	–16.53
Torsion–shear–bending moment	5a	190.5	141.4	–	–25.75
	5b	122.4	92.63	–	–24.30
	5c	207.7	158.1	–	–23.90
	5d	91.4	72.6	–	–20.59
	5e	188.6	145.8	–	–22.68
	5f	105.6	82.5	–	–21.90
	5g	151.9	111.6	–	–26.54
	5h	85.4	70.3	–	–17.74
	5i	189.6	145.8	–	–23.09
	5j	241.2	196.0	–	–18.75
	5k	253.3	210.5	–	–16.89
	5l	186.0	138.7	–	–25.44

interfaces are not generally known a priori [27]. However, when the eccentricity is a given parameter, as in the cases analyzed in this paper, the non-linear expressions can be solved in one-step.

Lastly, the torsion–shear–bending moment interaction resulted as a combination of the previous linear/linearized and non-linear formulations.

In order to be compared, experimental data are reported in absolute value on the relative yield domains (Fig. 8), while all the results are collected in Table 8.

The comparisons of the results obtained by the numerical model against experimental evidence show that the predicted yield domains agree well with the observed experimental results, to a small extent for the torsion–shear interaction. In fact, the experimental results were slightly greater than the numerical values for the pure shear and torsion moment represented by

“Linear/Linearized” models (Fig. 8b, c), relatively greater than those for the torsion–bending moment interaction expressed by “Non-Linear” model (Fig. 8e) and significantly for the torsion–shear interactions (Fig. 8d) and their combination with the bending moment.

Concerning the torsion–shear interaction, the tests results were in perfect agreement with the non-linear domain, which, therefore, can be considered experimentally validated. However, the results for the “Non-Linear” model were not reported in Table 8 (Sets 4a–f) since the comparison is mainly aimed at experimental validating the proposed linearized yield criteria. Thus, the expectable discrepancy between experimental and numerical results is due to the fact that the proposed linear approximation is too conservative with respect to the non-linear strength, as also evident in Fig. 8d. A piecewise linearization of the



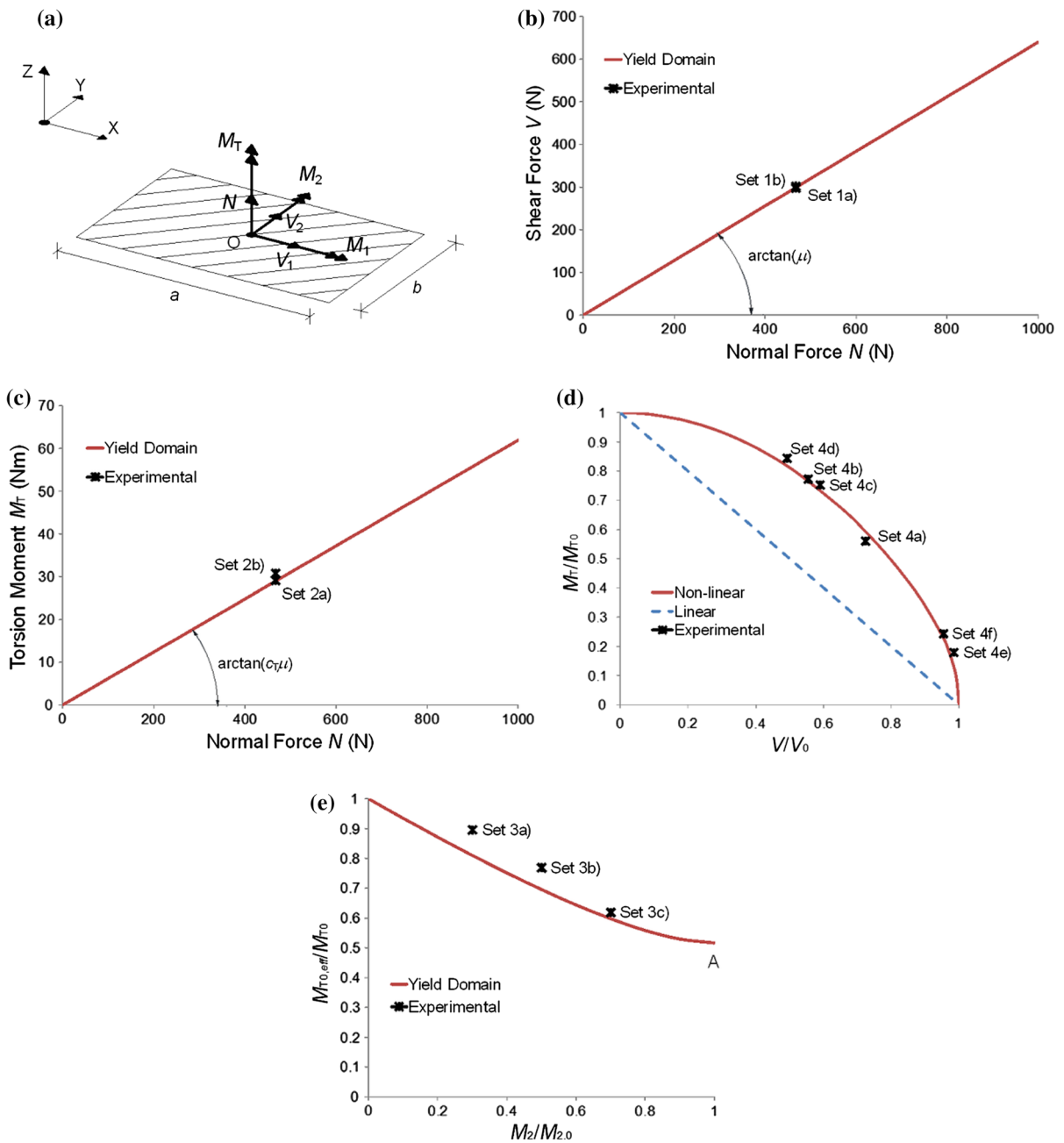


Fig. 8 Numerical model and yielding domains including experimental results (positive quadrants). **a** Static variables at the contact interface. **b** Yield domain for pure shear. **c** Yield

domain for pure torsion. **d** Non-dimensional torsion–shear interaction domains. **e** Non-dimensional torsion–bending moment interaction domain for $M_1 = 0$

non-linear curve is therefore necessary to reduce the differences observed.

On the other hand, the significant underestimation of the numerical results for the cases of torsion–shear–bending moments (Sets 5a–l) is mostly due to the

linear approximation of the torsion–shear interaction described above. For a more general case, also considering bending moments in both directions, the non-linearity of the torsion–bending moment interaction is expected to play an important role, too. Further



investigation is therefore required to improve the proposed models both to consider a piecewise linearization for torsion–shear interaction and to develop a reliable criterion for the linearization of the torsion–bending moment other than the iterative numerical procedure. However, the average percentage difference between all experimental and predicted shear forces was found to be about 17 %, and, overall, in favour of safety.

This comparison is useful, on the one hand, as a further validation the efficacy of the previously proposed yield domains in order to be used in 3D limit analysis formulations and, on the other, to highlight which yield domains need to be better represented.

5 Conclusions

Crucial to the limit analysis of 2D and 3D dry-jointed masonry block structures is a proper description of the constitutive laws that govern the frictional behaviour at contact interfaces. This topic is still poorly investigated in the literature.

The experimental programme carried out in this paper is focused on the definition of the yield domains for normal and shear forces, torsion and bending moments and their interactions, with reference to the single contact interface of a system composed of two dry-jointed tuff block. The testing device was designed and realized ad hoc since no standard equipments and procedures were found in the literature. The load was applied under displacement control at constant rate in order to make the results of several testing sets comparable each other.

The rather rigid-plastic behaviour of the frictional contact was captured by the load–displacement curves for all the tests and the forces corresponding to the first noticeable displacement were considered as the reference resistances.

The results of each set were then compared with those obtained by a recently proposed numerical model for 3D rigid block assemblages, under the assumptions of infinite compressive, shear and tensile strengths for blocks and no-tension and frictional behaviour at their contact. The comparisons show that the predicted yield domains agree well with the observed experimental results, to a small extent for the torsion–shear interaction and, as a partial

consequence, for the torsion–shear–bending moment interaction. However, the average percentage difference between all experimental and predicted shear forces was found to be about 17 %, and, overall, in favour of safety.

This comparison is useful, on the one hand, as a further validation of the efficacy of the previously proposed yield domains in order to be used in 3D limit analysis formulations and, on the other hand, to highlight which yield domains need to be better represented.

Besides, the testing device and the experimental campaign presented in this paper could be further validated by considering different pre-compression levels on the contact surface and other types of natural stones, considered representative of ancient masonry constructions. An interesting perspective may also be the development of the experimental equipment for the characterization of other masonry bonds, e.g., mortared joints, under the same loading combinations.

Acknowledgments The authors acknowledge the sponsorship of the Italian Civil Protection, through the RELUIS Project-Line: Masonry Structures (2015). The authors wish to express their gratitude to Dr. Carla Ceraldi, Mr. Mario Torricella and Mr. Domenico Imperatrice from the Laboratory of Architecture in Naples (DIST), for their assistance and support in the preparation of the specimens, test setup and throughout the execution of experimental investigations.

References

1. Atkinson RH, Amadei BP, Saeb S, Sture S (1989) Response of masonry and joints in direct shear. *J Struct Eng ASCE* 115(9):2276–2296
2. Baggio C, Trovalusi P (2000) Collapse behaviour of three-dimensional brick block systems using non-linear programming. *Struct Eng Mech* 10(2):181–195
3. Begg DW, Fishwick RJ (1995) Numerical analysis of rigid block structures including sliding. *Comput Methods Struct Mason* 3:177–183
4. Byerlee J (1978) Friction of rocks. *Pure Appl Geophys* 116:615–626
5. Casapulla C (1999) Frictional strength of out-of-plane loaded masonry walls. In: *Proceedings of the 9th national conference on seismic engineering in Italy*. ANIDIS, Torino, pp 1–12 (in Italian)
6. Casapulla C (2008) Lower and upper bounds in closed form for out-of-plane strength of masonry structures with frictional resistances. In: *Proceedings of the 6th international conference on structural analysis of historical constructions, SAHC08*, Bath, vol 2, pp 1191–1198
7. Casapulla C, D’Ayala D (2001) Lower bound approach to the limit analysis of 3D vaulted block masonry structures.



- Proceedings of the 5th international symposium on computer methods in structural masonry. STRUMAS V, Rome, pp 28–36
8. Casapulla C, Portioli F, Maione A, Landolfo R (2013) A macro-block model for in-plane loaded masonry walls with non-associative Coulomb friction. *Meccanica* 48(9):2107–2126
 9. Casapulla C, Cascini L, Portioli F, Landolfo R (2014) 3D macro and micro-block models for limit analysis of out-of-plane loaded masonry walls with non-associative Coulomb friction. *Meccanica* 49(7):1653–1678
 10. CEN (2002) EN 1052-3 European norm for methods of test for masonry—Part 3: determination of initial shear strength
 11. Copeland RE, Saxer EL (1964) Tests on structural bond of masonry mortars to concrete block. *J Am Concr I* 61(11):1411–1451
 12. Drucker DC (1954) Coulomb friction, plasticity and limit loads. *J Appl Mech* 21(1):71–74
 13. Feeny B, Guran A, Hinrichs N, Popp K (1998) A historical review on dry friction and stick-slip phenomena. *Appl Mech Rev* 51(5):321–341
 14. Ferris M, Tin-Loi F (2001) Limit analysis of frictional block assemblies as a mathematical program with complementarity constraints. *Int J Mech Sci* 43:209–224
 15. Gilbert M, Casapulla C, Ahmed HM (2006) Limit analysis of masonry block structures with non-associative frictional joints using linear programming. *Comput Struct* 84(13–14):873–887
 16. Hamid AA, Drysdale RG, Heidebrecht AC (1979) Shear strength of concrete masonry joints. *J Struct Div ASCE* 105:1227–1240
 17. Heyman J (1966) The stone skeleton. *Int J Solids Struct* 2:249–279
 18. Jukes P, Riddington JR (2001) The failure of brick triplet test specimens. *Mason Int* 15(1):30–33
 19. Kooharian A (1952) Limit analysis of voussoir (segmental) and concrete arches. *J Am Concr Inst* 24(4):317–328
 20. Lee HS, Park YJ, Cho TF, You KH (2001) Influence of asperity degradation on the mechanical behavior of rough rock joints under cyclic shear loading. *Int J Rock Mech Min Sci* 38:967–980
 21. Lourenço PB, Ramos LF (2004) Characterization of cyclic behavior of dry masonry joints. *J Struct Eng ASCE* 130(5):779–786
 22. Lourenço PB, Oliveira DV, Roca P, Orduña A (2005) Dry joint stone masonry walls subjected to in-plane combined loading. *J Struct Eng ASCE* 131(11):1665–1673
 23. Mihai LA (2010) A fixed-point approach to the limit load analysis of multibody structures with Coulomb friction. *Comput Struct* 88:859–869
 24. Oliveira DV (2003) Experimental and numerical analysis of blocky masonry structures under cyclic loading. PhD Thesis, University of Minho, Portugal
 25. Orduña A, Lourenço PB (2005a) Three-dimensional limit analysis of rigid blocks assemblages. Part I: torsion failure on frictional joints and limit analysis formulation. *Int J Solids Struct* 42(18–19):5140–5160
 26. Orduña A, Lourenço PB (2005b) Three-dimensional limit analysis of rigid blocks assemblages. Part II: load-path following solution procedure and validation. *Int J Solids Struct* 42(18–19):5161–5180
 27. Portioli F, Casapulla C, Cascini L, D’Aniello M, Landolfo R (2013a) Limit analysis by linear programming of 3D masonry structures with associative friction laws and torsion interaction effects. *Arch Appl Mech* 83(10):1415–1438
 28. Portioli F, Cascini L, Casapulla C, D’Aniello M (2013b) Limit analysis of masonry walls by rigid block modelling with cracking units and cohesive joints using linear programming. *Eng Struct* 57:232–247
 29. Portioli F, Casapulla C, Gilbert M, Cascini L (2014) Limit analysis of 3D masonry block structures with non-associative frictional joints using cone programming. *Comput Struct* 143:108–121
 30. Restrepo-Vélez LF, Magenes G, Griffith MC (2014) Dry stone masonry walls in bending—Part I: static tests. *Int J Archit Herit* 8(1):1–28
 31. Sassu M, Andreini M, Casapulla C, De Falco A (2013) Archaeological consolidation of UNESCO masonry structures in Oman: the Sumharam Citadel of Khor Rori and the Al-Balid Fortress. *Int J Archit Herit* 7(4):339–374
 32. Tran-Cao T (2009) Collapse analysis of block structures in frictional contact. PhD Thesis, The University of New South Wales, Sydney
 33. van der Pluijm R (1999) Out of plane bending of masonry behaviour. PhD Thesis, Eindhoven University of Technology, The Netherlands
 34. Vasconcelos G, Lourenço PB (2009) Experimental characterization of stone masonry in shear and compression. *Constr Build Mater* 23:3337–3345
 35. Villemus B, Morel JC, Boutin C (2007) Experimental assessment of dry stone retaining wall stability on a rigid foundation. *Eng Struct* 29(9):2124–2132
 36. Zuccarello FA, Milani G, Olivito RS, Tralli A (2009) A numerical and experimental analysis of unbonded brickwork panels laterally loaded. *Constr Build Mater* 23:2093–2106